Sudden change from chaos to oscillation death in the Bonhoeffer–van der Pol oscillator under weak periodic perturbation

Munehisa Sekikawa*
Institute of Industrial Science, The University of Tokyo, 153-8505 Tokyo, Japan

Kuniyasu Shimizu
Department of Electrical, Electronics and Computer Engineering, Chiba Institute of Technology, 275-0016 Chiba, Japan

Naohiko Inaba
Organisation for the Strategic Coordination of Research and Intellectual Property, Meiji University, 214-8571 Kawasaki, Japan

Hiroki Kita and Tetsuro Endo
Department of Electronics and Bioinformatics, Meiji University, 214-8571 Kawasaki, Japan

Ken'ichi Fujimoto and Tetsuya Yoshinaga
Institute of Health Biosciences, The University of Tokushima, 770-8509 Tokushima, Japan

Kazuyuki Aihara
Aihara Innovative Mathematical Modelling Project, FIRST, JST, 153-8505 Tokyo, Japan and Institute of Industrial Science, The University of Tokyo, 153-8505 Tokyo, Japan

(Received 10 May 2011; revised manuscript received 3 August 2011; published 10 November 2011)

In this paper, we analyze the sudden change from chaos to oscillation death generated by the Bonhoeffer–van der Pol (BVP) oscillator under weak periodic perturbation. The parameter values of the BVP oscillator are chosen such that a stable focus and a stable relaxation oscillation coexist if no perturbation is applied. In such a system, complicated bifurcation structure is expected to emerge when weak periodic perturbation is applied because the stable focus and the stable relaxation oscillation coexist in close proximity in the phase plane. We draw a bifurcation diagram of the fundamental harmonic entrainment. The bifurcation structure is complex because there coexist two bifurcation sets. One is the bifurcation set generated in the vicinity of the stable focus, and the other is that generated in the vicinity of the stable relaxation oscillation. By analyzing the bifurcation diagram in detail, we can explain the sudden change from chaos with complicated waveforms to oscillation death. We make it clear that this phenomenon is caused by a saddle-node bifurcation.

DOI: 10.1103/PhysRevE.84.056209 PACS number(s): 05.45.Ac

I. INTRODUCTION

The Bonhoeffer–van der Pol (BVP) oscillator is known as a simplified Hodgkin-Huxley model that shows qualitatively similar behavior with "squid giant axons," and chaos generated by the driven BVP oscillator has been studied intensively [1–9]. The autonomous BVP oscillator exhibits an interesting bifurcation structure compared with the van der Pol oscillator. The BVP oscillator contains a resistor in series with the inductor. It is pointed out by Rabinovitch *et al*. [10,11] that the BVP oscillator possesses richer dynamics than the van der Pol oscillator because a subcritical Andronov-Hopf bifurcation (AHB) can occur in the BVP oscillator due to the presence of the resistor, whereas only a supercritical AHB is possible in the van der Pol oscillator. A stable focus and a stable relaxation oscillation coexist in close proximity in the phase plane near a subcritical AHB point.

How is the circuit dynamics influenced by weak periodic perturbation in such a system, where a stable focus and a stable relaxation oscillation coexist in close proximity when no perturbation is applied? Complicated bifurcation structure can be expected to emerge in this dynamical system since the solution can alternate between the stable focus and the stable relaxation oscillation. So far, a system without a forcing term [10], or only a periodic response in a system with a forcing term of order 1 [11], has been studied.

To make the influence of weak periodic perturbation clear, we conducted numerical studies for such a weakly driven BVP oscillator [12]. As a result, we found complicated mixed-mode oscillations (MMOs) and chaos in this oscillator. Note that the noteworthy simplicity of the electric circuit nevertheless generates such complex dynamics. However, MMOs and chaos are just examples of possible complex phenomena generated in this electric circuit model. The dynamical circuit, which was proposed in Ref. [12], is considered to be a minimal model that exhibits extremely complicated behavior, where complex MMOs that consist of various MMO sequences and chaos with "intermittency MMOs" [12] are observed.

In this paper, we further investigate the BVP oscillator under weak periodic perturbation in detail. We study the bifurcation structure near the fundamental harmonic synchronization region. The MMOs, as Shimizu *et al*. have observed [12], correspond to the periodic oscillations in the higher-harmonic

*sekikawa@sat.t.u-tokyo.ac.jp

synchronization regions. In the fundamental harmonic synchronization region, we discover a sudden change from a chaotic oscillation to oscillation death [13,14]. Strictly speaking, oscillation death here is not a stable equilibrium but a very weak oscillation because a weak forcing term exists in the oscillator. We call this phenomenon "oscillation death in a nonautonomous oscillator" because chaotic oscillation suddenly vanishes by this bifurcation and drastically arrives at an extremely weak oscillation. We confirm numerically that the stable relaxation oscillation vanishes with very weak perturbation. Weak external periodic perturbation can both delete the coexisting stable limit cycle and maintain the coexisting stable focus point; it can also delete the coexisting stable focus point and maintain the coexisting stable limit cycle. This phenomenon can be considered as a control of the coexisting stable state using weak periodic perturbation.

We draw a two-parameter bifurcation diagram especially in order to make clear the mechanism of the sudden change from chaos to oscillation death. The bifurcation diagram is complex because there are two attractive regions, that is, one of the stable relaxation oscillation and the other of the stable focus. The former bifurcation structure is rather simple because the synchronization region is a well-known Arnold tongue. On the other hand, the latter is complicated and consists of saddle-node bifurcation curves, period-doubling bifurcation curves, and Neimark-Sacker bifurcation curves. When we superpose the bifurcation set of the stable relaxation oscillation and that of the stable focus, we can find the mechanism of the sudden change from the chaotic oscillation to oscillation death in a nonautonomous oscillator. This phenomenon is caused by the saddle-node bifurcation of the latter bifurcation set.

II. PRELIMINARY STUDY OF THE BVP OSCILLATOR

In this section, we study the BVP oscillator when no perturbation is applied. Figure 1 shows the circuit diagram of the BVP oscillator. The electric circuit consists of one capacitor C, one inductor L, one linear resistor R, one voltage source E_0, and only one nonlinear negative conductance G. The v-i characteristics of the nonlinear conductance is assumed to be expressed by the third-order polynomial function as follows:

$$g(v) = -g_1 v + g_3 v^3 \quad (g_1 > 0,\ g_3 > 0). \tag{1}$$

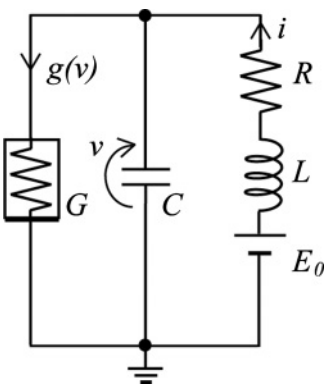

FIG. 1. Circuit diagram of the Bonhoeffer–van der Pol oscillator.

It should be noted that Rabinovitch *et al.* point out that subcritical AHB can take place in the presence of the linear resistor R in the BVP oscillator [10,11].

From Kirchhoff's law, the governing equations of the electric circuit are represented as follows:

$$\begin{aligned} C\frac{dv}{dt} &= i - g(v), \\ L\frac{di}{dt} &= -v - iR + E_0, \end{aligned} \tag{2}$$

where the capacitance C is assumed to be small. In this case, the circuit dynamics is described as a slow-fast system. By changing variables and constants as follows:

$$\begin{aligned} &\varepsilon = \frac{C}{g_1^2 L}, \quad k_1 = g_1 R, \quad B_0 = \sqrt{\frac{g_3}{g_1}}E_0, \\ &t = g_1 L\tau, \quad \frac{d}{d\tau} = \cdot, \quad x = \sqrt{\frac{g_3}{g_1}}v, \quad y = \sqrt{\frac{g_3}{g_1^3}}i, \end{aligned} \tag{3}$$

the normalized version of Eqs. (2) is derived as follows:

$$\begin{aligned} \varepsilon\dot{x} &= y - (-x + x^3), \\ \dot{y} &= -x - k_1 y + B_0. \end{aligned} \tag{4}$$

ε is a small parameter that corresponds to C. Throughout this study, we set $\varepsilon = 0.1$.

Figure 2 shows the one-parameter bifurcation diagram, where the abscissa denotes the parameter B_0 and the ordinate denotes the state variable x. In this figure, we set $k_1 = 0.2$. The thin (red) solid line and dashed (blue) line denote a stable focus and an unstable focus, respectively. The filled circles denote the minimum and maximum values of x in a limit cycle. By varying B_0, an AHB takes place at $B_0 = B_0^c \simeq 0.494\,56$. The AHB is clearly supercritical. A sudden change of the size in the limit cycle is well known as the "canard explosion" in the slow-fast systems. To summarize, (a) only one stable focus exists for $B_0 > B_0^c$, and (b) an unstable focus and a stable limit cycle coexist for $B_0 < B_0^c$. The attractor is only the limit cycle in the region.

According to numerical study, it has been clarified that the subcritical AHB can take place when k_1 becomes large.

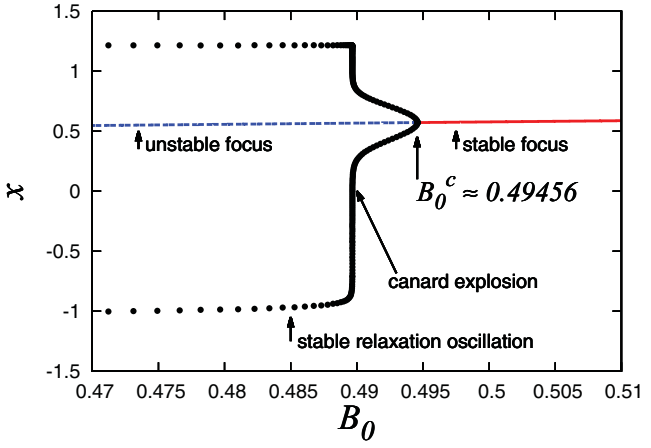

FIG. 2. (Color online) One-parameter bifurcation diagram near a supercritical AHB point ($k_1 = 0.2$).

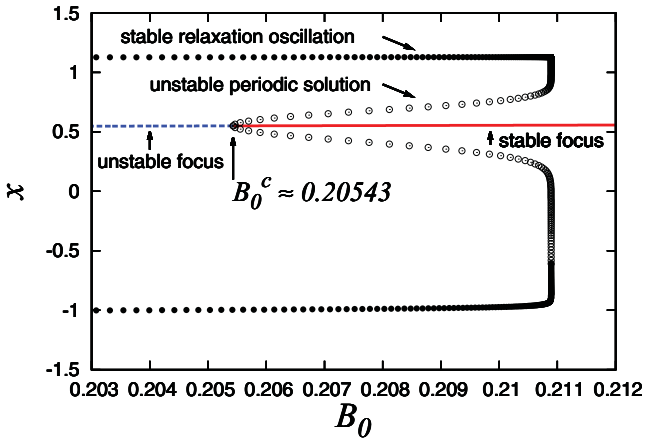

FIG. 3. (Color online) One-parameter bifurcation diagram near a subcritical AHB point ($k_1 = 0.9$).

Figure 3 shows the one-parameter bifurcation diagram for $k_1 = 0.9$, where the open circles denote the maximum and minimum values of x in an unstable limit cycle and the filled circles represent those in a stable limit cycle. To summarize in this case, (a′) only one stable focus exists for $B_0 >\sim 0.211$ ($\equiv B_0^f$); (b′) a stable focus, a stable relaxation oscillation, and an unstable limit cycle coexist for $B_0^c < B_0 < B_0^f$ (note that two attractors coexist in this region); and (c′) an unstable focus and a stable relaxation oscillation coexist for $B_0 < B_0^c$. The attractor is the stable relaxation oscillation only.

We are interested in the case of (b′). Figure 4 shows the attractors and the unstable limit cycle in the phase plane when the parameters are set at $k_1 = 0.9$ and $B_0 = 0.21$. A stable focus is plotted with a filled circle, a stable relaxation oscillation is drawn with a solid (red) line, and an unstable limit cycle is illustrated with a dashed (blue) line. Also the nullclines are drawn by solid (black) lines in Fig. 4. From the figure, we can find that the stable focus and the stable relaxation oscillation coexist in close proximity.

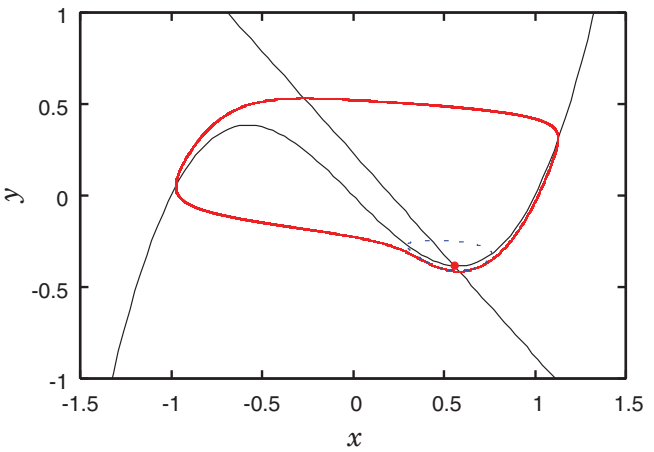

FIG. 4. (Color online) Coexisting stable focus (filled circle), unstable limit cycle (dashed line), and stable relaxation oscillation (solid line) ($k_1 = 0.9, B_0 = 0.21$).

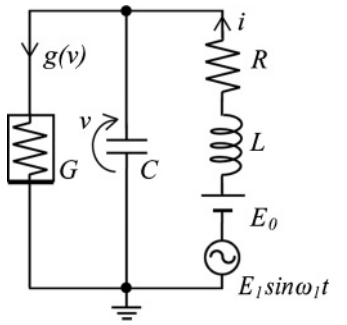

FIG. 5. The BVP oscillator under weak periodic perturbation.

III. PHENOMENA OBSERVED IN THE BVP OSCILLATOR UNDER WEAK PERIODIC PERTURBATION

In the previous section, we pointed out that a bistability exists near the subcritical AHB point, where a stable focus and a stable relaxation oscillation coexist in close proximity in the phase plane.

How does the influence of weak periodic perturbation effect the dynamics? In such a case, the solution may alternate between the stable focus and the stable relaxation oscillation due to perturbation, and it is expected that complicated

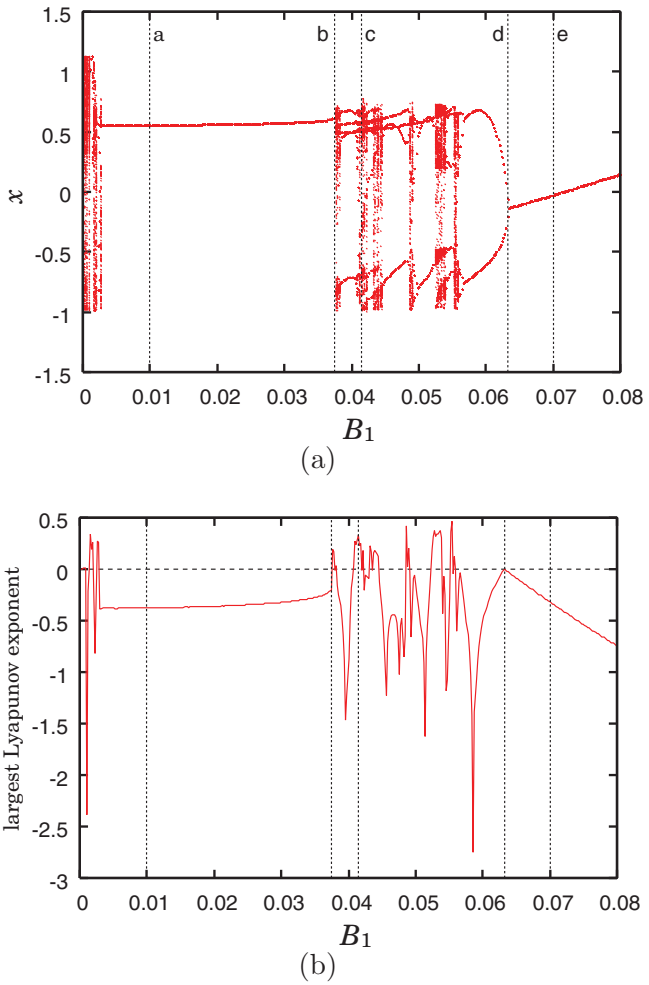

FIG. 6. (Color online) One-parameter bifurcation diagram of T_{B_1} and the corresponding largest Lyapunov exponent.

behavior is generated. The dynamical model is presented in Fig. 5. Shimizu *et al*. analyzed this dynamics and found various types of MMOs, including extremely complicated MMOs previously unreported [12].

We further analyze this model near the fundamental harmonic synchronization region for the stable relaxation oscillation. The governing equations of the electric circuit are represented as follows:

$$\begin{aligned} \varepsilon \dot{x} &= y - (-x + x^3), \\ \dot{y} &= -x - k_1 y + B_0 + B_1 \sin \omega\tau, \end{aligned} \tag{5}$$

where

$$B_1 = \sqrt{\frac{g_3}{g_1}} E_1, \quad \omega = L g_1 \omega_1, \tag{6}$$

and B_1 is assumed to be small.

We set $k_1 = 0.9$ and $B_0 = 0.21$ in the following analysis. In this case, a stable focus and a stable relaxation oscillation coexist when $B_1 = 0$, as shown in Fig. 4. We integrated the equations numerically using the fourth-order Runge-Kutta method with a step size of $2\pi/\omega/1024$ throughout this study.

Let us set $\omega = 1.35$ and investigate the dynamics by varying the parameter B_1. Since the perturbation is assumed to be periodic, the Poincaré mapping T_{B_1} of Eqs. (5) can be defined as follows:

$$\begin{aligned} &T_{B_1}: R^2 \to R^2 \\ &(x,y)^\top \mapsto T_{B_1}(x,y)^\top \equiv \varphi(2\pi/\omega;\ (x,y)^\top,\ B_1), \end{aligned} \tag{7}$$

where the superscript $\top$ denotes the transpose of the vector, $\varphi(t)$ is the solution, and B_1 is the bifurcation parameter.

Figure 6 shows a one-parameter bifurcation diagram of the Poincaré mapping T_{B_1} and the corresponding largest Lyapunov exponent. The abscissa denotes the parameter B_1, and the ordinates of Figs. 6(a) and 6(b) denote x of the Poincaré mapping and the corresponding largest Lyapunov exponent, respectively. The exponent is calculated by an algorithm produced by Shimada and Nagashima [15].

According to the numerical results, a quasiperiodic attractor is generated as a result of extremely small B_1. This situation is reasonable from the results of other periodically driven oscillators [16]. An example of the attractor at $B_1 = 0.0008$ is presented in Fig. 7. We check the quasiperiodicity of this attractor by calculating the largest Lyapunov exponent. Also, we find that chaos is generated when B_1 is still very small. The chaotic attractor with $B_1 = 0.002$ is presented in Fig. 8. Sekikawa *et al*. pointed out that chaos appears even if the

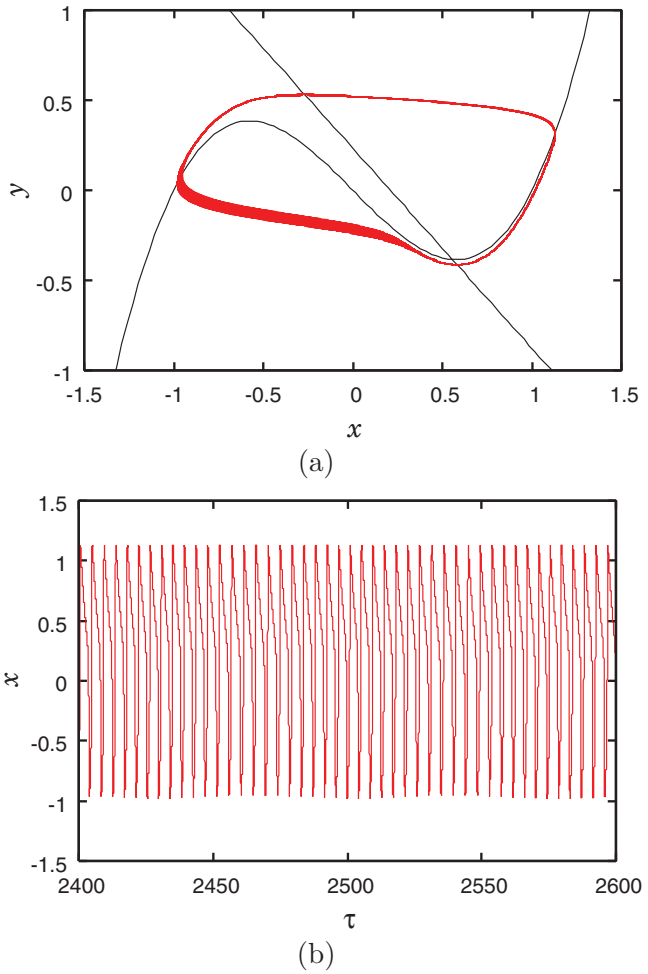

FIG. 7. (Color online) Quasiperiodic attractor ($B_1 = 0.0008$). (a) The attractor in the phase plane. (b) Time series.

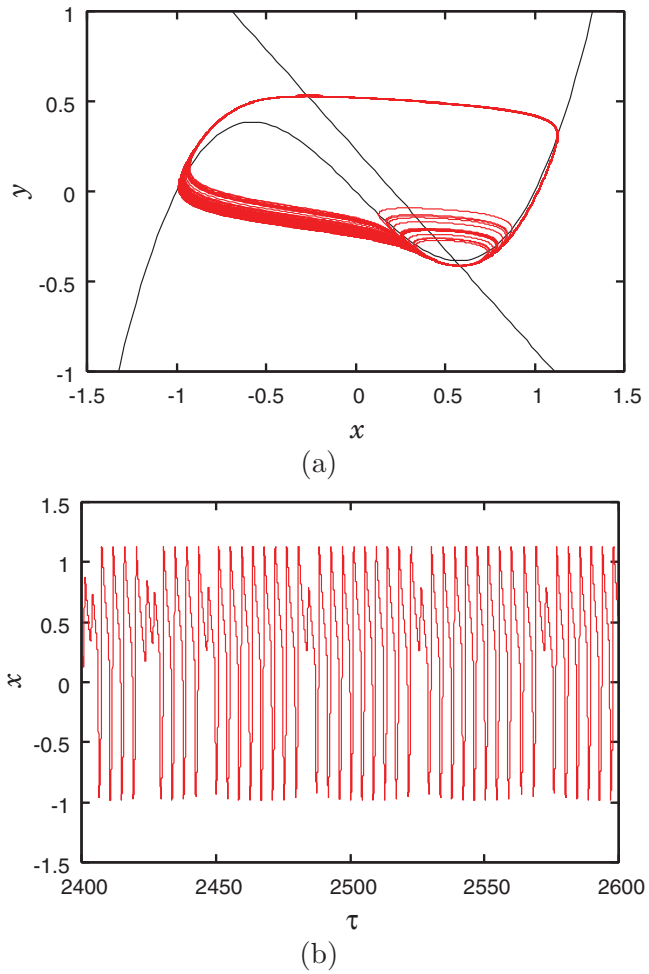

FIG. 8. (Color online) Chaotic attractor for small B_1 ($B_1 = 0.002$). (a) The attractor in the phase plane. (b) Time series.

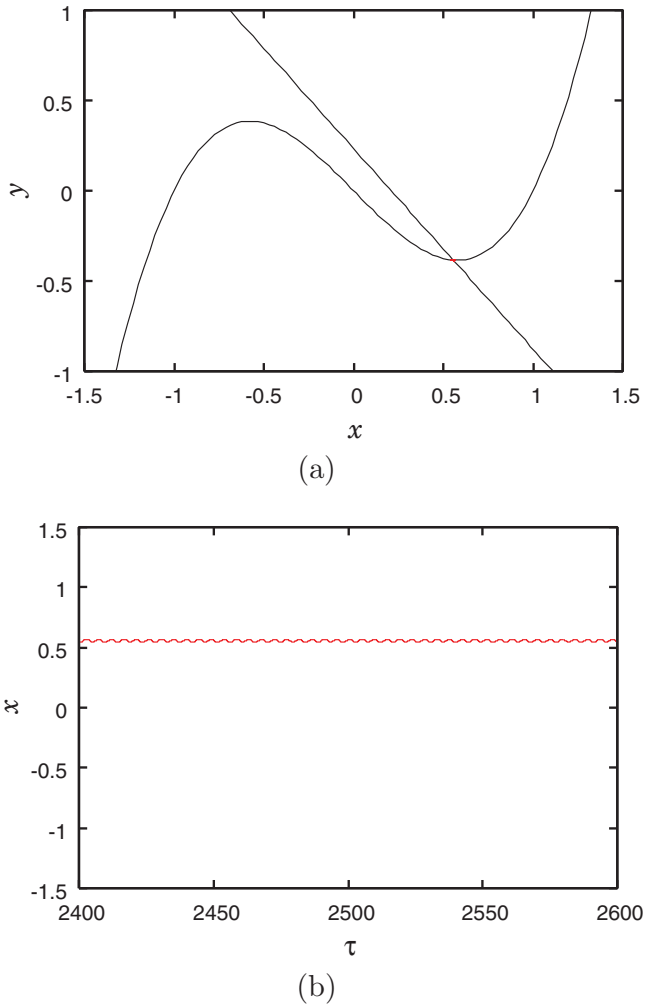

FIG. 9. (Color online) Oscillation death ($B_1 = 0.01$). (a) The attractor in the phase plane. (b) Time series.

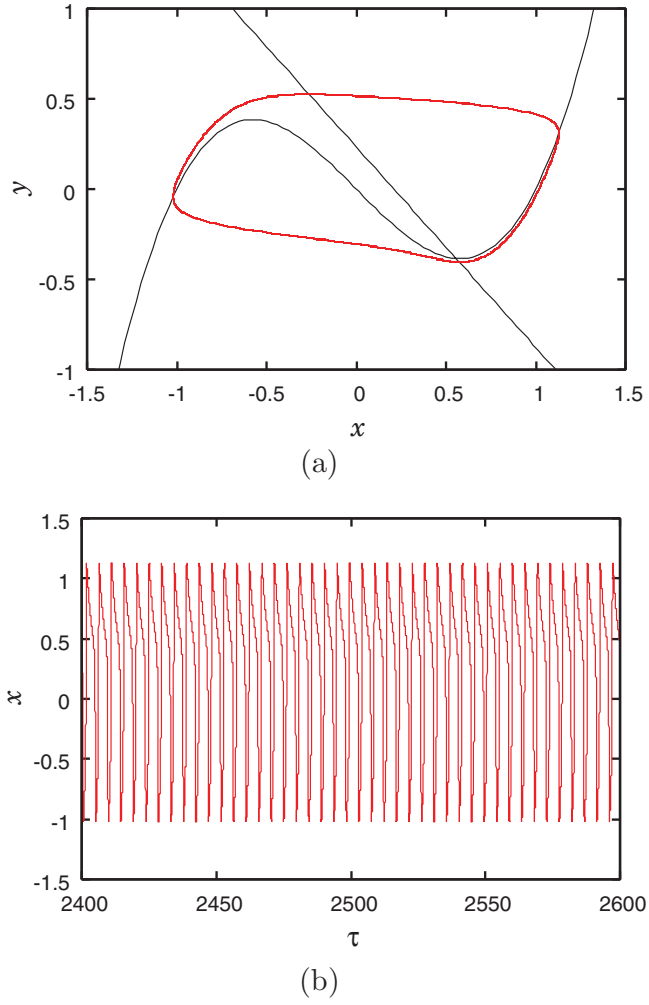

FIG. 10. (Color online) Stable relaxation oscillation ($B_1 = 0.07$). (a) The attractor in the phase plane. (b) Time series.

amplitude of the forcing term is very small in slow-fast systems [17,18].

In Fig. 6, periodic attractors exist in wide ranges of the parameter value of B_1. One is generated in the region around "a" in the figure, and another is generated in the region around "e." Sandwiched between these two periodic regions, chaotic oscillations are observed, most notably near "c" in Fig. 6.

A remarkable difference can be found, however, for these two periodic regions. Figure 9(a) shows the solution in the phase plane observed at "a" in Fig. 6. The solution stays near a stable focus. Strictly speaking, since the system is weakly driven, an extremely small oscillation exists. We call this phenomenon "oscillation death in a nonautonomous oscillator" because chaotic oscillation suddenly vanishes due to a bifurcation and drastically arrives at an extremely weak oscillation. The time series is shown in Fig. 9(b). We set the initial condition at various points, especially at outer points of the stable relaxation oscillation. These numerical results show that the stable relaxation oscillation disappears due to weak periodic perturbation. In contrast to oscillation death, a stable relaxation oscillation is observed at the parameter value marked with "e" in Fig. 6 as shown in Fig. 10, where the attractor near the stable focus disappears. Also, a chaotic oscillation observed at "c" in Fig. 6 is presented in Fig. 11. The time series of this chaotic attractor is very complex, as shown in Fig. 11(b). The solution crosses over the unstable periodic orbit frequently and alternates between the stable focus and the stable relaxation oscillation.

A remarkable phenomenon is observed at "b" in Fig. 6. At this point, a sudden change from chaos to oscillation death is observed. It is noteworthy that such a simple second-order oscillator under weak periodic perturbation exhibits extremely complicated behavior.

IV. BIFURCATION ANALYSIS FOR THE FUNDAMENTAL HARMONIC ENTRAINMENT

To analyze the mechanism of the observed phenomena in detail, we draw a two-parameter bifurcation diagram near the fundamental harmonic entrainment for the stable relaxation oscillation that exists when no perturbation is applied. The bifurcation structure is complex because two bifurcation sets and a different attractor coexist when perturbation is weak. One is a bifurcation set that originates from the stable relaxation oscillation, and the other is one that originates from the stable focus.

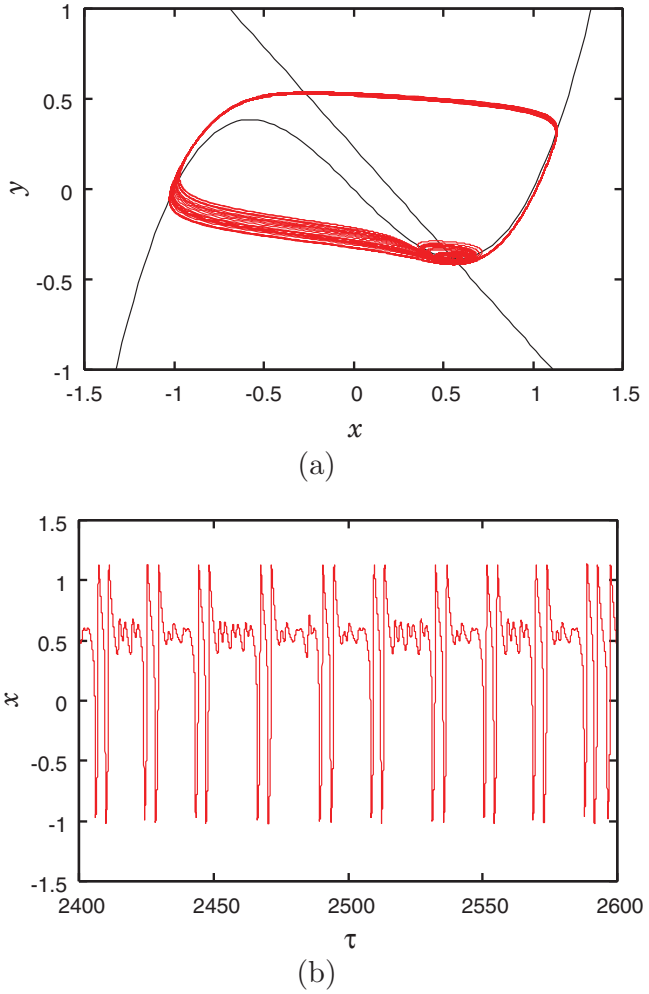

FIG. 11. (Color online) Chaotic oscillation ($B_1 = 0.0415$). (a) The attractor in the phase plane. (b) Time series.

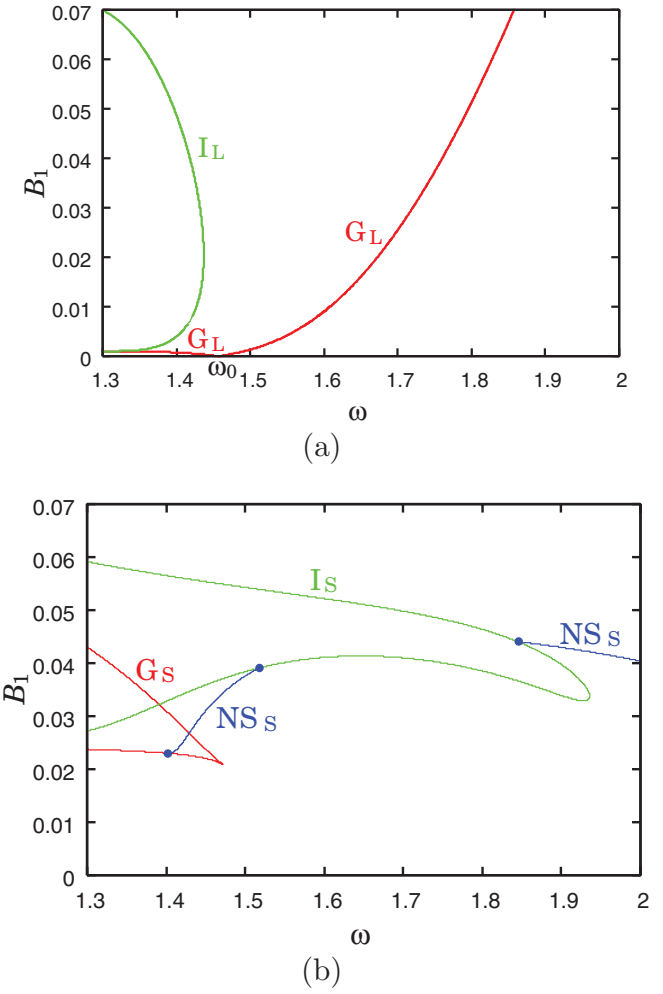

FIG. 12. (Color online) Two-parameter bifurcation diagrams. (a) Bifurcation sets related to the stable relaxation oscillation. (b) Bifurcation sets related to the stable focus.

Figure 12 shows these bifurcation sets. These bifurcation sets are calculated by the shooting algorithm proposed by Kawakami [19]. The bifurcation structure of Fig. 12(a) is rather simple because it consists of a synchronization region that is well known as the Arnold tongue. From simulation, the angular frequency of the stable relaxation oscillation when $B_1 = 0$ is estimated to be $\omega \simeq 1.4571$ ($\equiv \omega_0$). In this diagram, the fundamental harmonic synchronization region, which is surrounded by two saddle-node bifurcation curves denoted by G_L and a period-doubling bifurcation curve I_L, exist. The bifurcation structure of Fig. 12(b) is more complex. It consists of a saddle-node bifurcation curve G_S, a period-doubling bifurcation curve I_S, and Neimark-Sacker bifurcation curves NS_S.

By superimposing Figs. 12(a) and 12(b), the mechanism of sudden change from chaos to oscillation death becomes clear. Figure 13 shows the superimposed bifurcation diagram. The regions where the largest Lyapunov exponent is positive are shaded in the figure. Note that the initial point is chosen as $(x_0, y_0) = (0.555, 2)$, which is located at the outer side of the stable relaxation oscillation that exists when no perturbation is applied.

The phenomena of Fig. 6 are observed along the long and short dashed line in Fig. 13. Moving down this line from above, a stable relaxation oscillation (Fig. 10) is observed at a point "e," and the period-doubling bifurcation accumulation begins at the point "d." Then, chaos in Fig. 11 is observed at "c." A

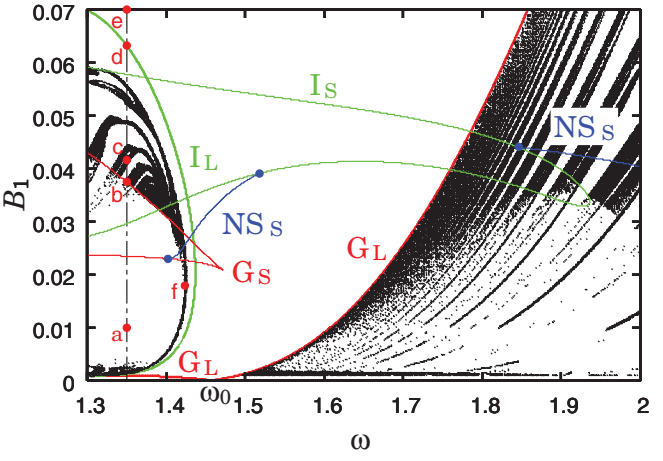

FIG. 13. (Color online) The superimposed bifurcation diagram.

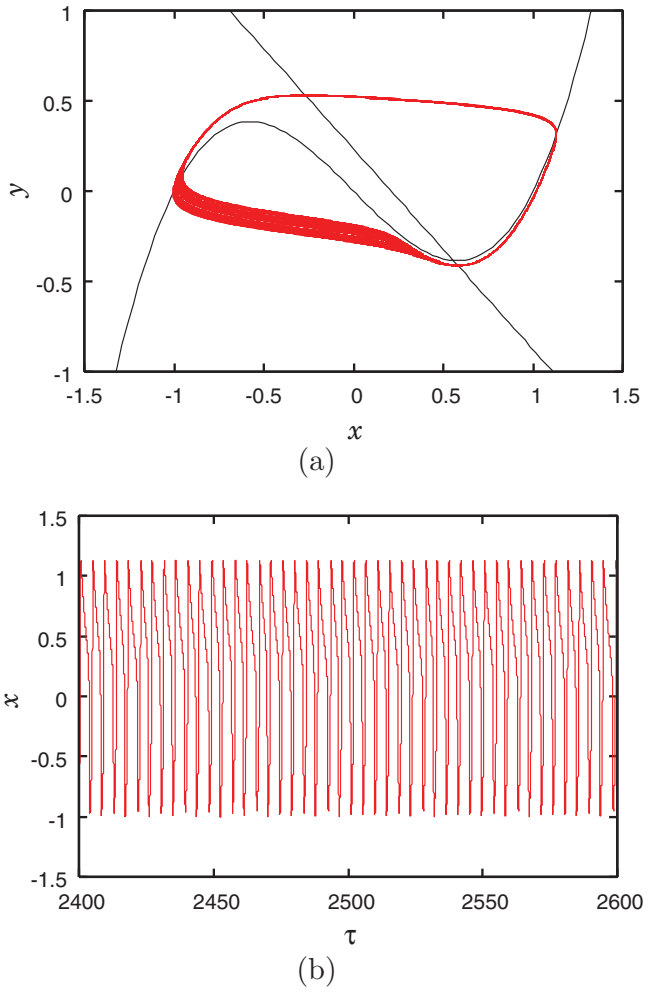

FIG. 14. (Color online) Chaotic oscillation ($\omega = 1.424$, $B_1 = 0.018$). (a) The attractor in the phase plane. (b) Time series.

sudden change from chaos to oscillation death takes place at the point "b." Therefore, the oscillation death is caused by the saddle-node bifurcation G_S.

On the other hand, an interesting chaotic oscillation is observed at a point "f." The attractor in the phase plane and the time series are shown in Figs. 14(c) and 14(b), respectively. This phenomenon is caused after the accumulation of period-doubling bifurcations of the stable relaxation oscillation. Therefore, this attractor should be chaotic. From the time series and the behavior in the phase plane, at first glance, this phenomenon seems to be a stable relaxation oscillation or a quasiperiodic one. It is confirmed, however, that this attractor is chaotic due to the largest Lyapunov exponent.

V. CONCLUSION

In this paper, we analyzed a simple electric circuit that exhibits extremely complicated behavior. A sudden change from chaos to oscillation death in a nonautonomous oscillator was observed. We drew a two-parameter bifurcation diagram near the fundamental harmonic synchronization region and clarified the mechanism of this complicated phenomenon. Since the dynamical circuit we have proposed was remarkably simple, the phenomena we have observed in this dynamical system could be widely observed in other slow-fast dynamical systems.

ACKNOWLEDGMENTS

This research is partially supported by the Aihara Innovative Mathematical Modelling Project, the Japan Society for the Promotion of Science (JSPS) through the "Funding Program for World-Leading Innovative R&D on Science and Technology (FIRST Program)," initiated by the Council for Science and Technology Policy (CSTP).

APPENDIX A: BRIEF EXPLANATION ON CALCULATION OF THE BIFURCATION PARAMETER VALUES

In this Appendix, Kawakami's shooting algorithm to obtain bifurcation boundaries [19] is briefly explained. Let Eqs. (5) be expressed by

$$\dot{\boldsymbol{x}} = \boldsymbol{f}(\boldsymbol{x}, \tau), \tag{A1}$$

where $\boldsymbol{x} = (x, y)^\top$. The Poincaré mapping is expressed by T_λ, where λ is a parameter. Let $\boldsymbol{u} = (u, v)^\top$ be an m-periodic point of T_λ. Then $\boldsymbol{u}$ satisfies

$$\mathrm{T}_\lambda^m(\boldsymbol{u}) - \boldsymbol{u} = 0, \tag{A2}$$

where T_λ^m is the m-times composite map of T_λ. The characteristic equation of $\boldsymbol{u}$ is given by the following equation:

$$\left| \frac{\partial}{\partial \boldsymbol{u}} \mathrm{T}_\lambda^m(\boldsymbol{u}) - \mu \boldsymbol{I} \right| = 0, \tag{A3}$$

where $\boldsymbol{I}$ is the unit matrix and μ is an eigenvalue. The bifurcation parameter of a saddle-node bifurcation, a period-doubling bifurcation, and a Neimark Sacker bifurcation is obtained by setting the eigenvalue parameter μ at 1, -1, and $e^{j\theta}$, respectively, and solving Eqs. (A2) and (A3) simultaneously for $\boldsymbol{u}$ and λ. In actual calculation, these simultaneous equations can be solved by Newton Raphson method.

The derivatives of Poincaré mapping T_λ with respect to the periodic point $\boldsymbol{u}$ and the parameter λ can be obtained partly from the following variational equations with respect to the initial values of $\boldsymbol{u}$ and λ:

$$\begin{aligned}
\frac{\partial}{\partial \boldsymbol{u}} \mathrm{T}_\lambda^m(\boldsymbol{u}) &= \frac{\partial}{\partial \boldsymbol{u}} \boldsymbol{\varphi}(2m\pi/\omega, \boldsymbol{u}, \lambda), \\
\frac{\partial}{\partial \lambda} \mathrm{T}_\lambda^m(\boldsymbol{u}) &= \frac{\partial}{\partial \lambda} \boldsymbol{\varphi}(2m\pi/\omega, \boldsymbol{u}, \lambda), \\
\frac{\partial^2}{\partial u^2} \mathrm{T}_\lambda^m(\boldsymbol{u}) &= \frac{\partial^2}{\partial u^2} \boldsymbol{\varphi}(2m\pi/\omega, \boldsymbol{u}, \lambda), \\
\frac{\partial^2}{\partial u \partial \lambda} \mathrm{T}_\lambda^m(\boldsymbol{u}) &= \frac{\partial^2}{\partial u \partial \lambda} \boldsymbol{\varphi}(2m\pi/\omega, \boldsymbol{u}, \lambda),
\end{aligned} \tag{A4}$$

where $\boldsymbol{\varphi}(0, \boldsymbol{u}, \lambda) = \boldsymbol{u}$ is assumed. The right-hand side of Eqs. (A4) can be obtained by integrating the equations as follows:

$$\frac{d}{d\tau}\frac{\partial \boldsymbol{\varphi}}{\partial \boldsymbol{u}} = \frac{\partial \boldsymbol{f}}{\partial \boldsymbol{x}}\frac{\partial \boldsymbol{\varphi}}{\partial \boldsymbol{u}}, \quad \text{where} \quad \left.\frac{\partial \boldsymbol{\varphi}}{\partial \boldsymbol{u}}\right|_{\tau=0} = \mathbf{I},$$

$$\frac{d}{d\tau}\frac{\partial \boldsymbol{\varphi}}{\partial \lambda} = \frac{\partial \boldsymbol{f}}{\partial \boldsymbol{x}}\frac{\partial \boldsymbol{\varphi}}{\partial \lambda} + \frac{\partial \boldsymbol{f}}{\partial \lambda}, \quad \text{where} \quad \left.\frac{\partial \boldsymbol{\varphi}}{\partial \lambda}\right|_{\tau=0} = 0,$$

$$\frac{d}{d\tau}\frac{\partial^2\boldsymbol{\varphi}}{\partial u^2} = \frac{\partial \boldsymbol{f}}{\partial \boldsymbol{x}}\frac{\partial^2\boldsymbol{\varphi}}{\partial u^2} + \frac{\partial}{\partial u}\left(\frac{\partial \boldsymbol{f}}{\partial \boldsymbol{x}}\right)\frac{\partial\boldsymbol{\varphi}}{\partial u}, \tag{A5}$$

$$\frac{d}{d\tau}\frac{\partial^2\boldsymbol{\varphi}}{\partial u\partial\lambda} = \frac{\partial \boldsymbol{f}}{\partial \boldsymbol{x}}\frac{\partial^2\boldsymbol{\varphi}}{\partial u\partial\lambda} + \frac{\partial}{\partial u}\left(\frac{\partial \boldsymbol{f}}{\partial \boldsymbol{x}}\right)\frac{\partial\boldsymbol{\varphi}}{\partial\lambda} + \frac{\partial}{\partial u}\left(\frac{\partial \boldsymbol{f}}{\partial\lambda}\right),$$

where

$$\left.\frac{\partial^2\boldsymbol{\varphi}}{\partial u^2}\right|_{\tau=0}=0,$$

$$\left.\frac{\partial^2\boldsymbol{\varphi}}{\partial u\partial\lambda}\right|_{\tau=0}=0,$$

$$\frac{\partial}{\partial u}\left(\frac{\partial \boldsymbol{f}}{\partial x}\right)=\left(\frac{\partial^2 \boldsymbol{f}}{\partial x^2}\quad\frac{\partial^2 \boldsymbol{f}}{\partial x\partial y}\right)\frac{\partial\boldsymbol{\varphi}}{\partial u}, \tag{A6}$$

$$\frac{\partial}{\partial u}\left(\frac{\partial \boldsymbol{f}}{\partial y}\right)=\left(\frac{\partial^2 \boldsymbol{f}}{\partial x\partial y}\quad\frac{\partial^2 \boldsymbol{f}}{\partial y^2}\right)\frac{\partial\boldsymbol{\varphi}}{\partial u},$$

$$\frac{\partial}{\partial u}\left(\frac{\partial \boldsymbol{f}}{\partial\lambda}\right)=\left(\frac{\partial^2 \boldsymbol{f}}{\partial x\partial\lambda}\quad\frac{\partial^2 \boldsymbol{f}}{\partial y\partial\lambda}\right)\frac{\partial\boldsymbol{\varphi}}{\partial u}.$$

These variational equations can be obtained by differentiating Eq. (A7) with $\boldsymbol{u}$ or λ as many times as needed:

$$\frac{d}{d\tau}\boldsymbol{\varphi}(\tau,\boldsymbol{u},\lambda) = \boldsymbol{f}(\boldsymbol{\varphi}(\tau,\boldsymbol{u},\lambda),\tau), \quad \text{where} \quad \boldsymbol{\varphi}(0,\boldsymbol{u},\lambda) = \boldsymbol{u}. \tag{A7}$$

APPENDIX B: STRUCTURE OF THE FIXED-POINT MANIFOLD

In this appendix, we show how the fixed-point manifold [20] is formed in the two-parameter bifurcation diagram of Fig. 12(b). The fixed-point manifold is a set (x,y,B_1) that satisfies $T_{B_1}(x,y)^\top - (x,y)^\top = (0,0)^\top$. Referring to the notation of Ref. [21], hyperbolic fixed points are expressed by ${}_kD(k=0,1,2)$ and ${}_kI(k=1)$, where D and I denote the type of fixed points and the subscript integer indicates the dimension of unstable subspace.

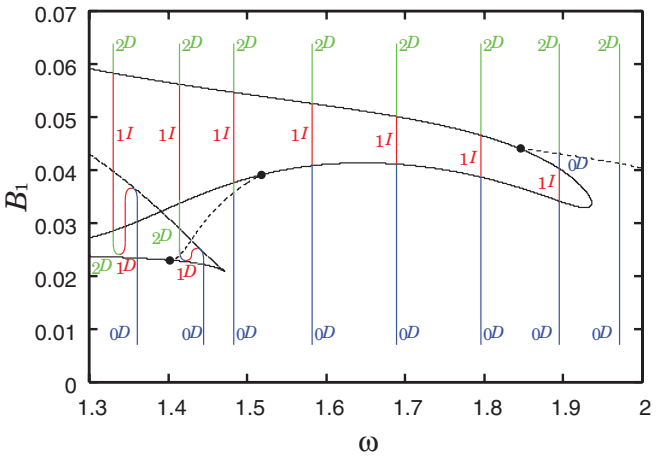

FIG. 15. (Color online) Structure of the fixed-point manifold of Fig. 12(b).

Figure 15 shows the structure of the fixed-point manifold of Fig. 12(b). From the calculated two-parameter bifurcation diagram and its fixed-point manifold, we can theoretically explain the disappearance of "small-amplitude oscillation" for larger parameter values B_1. It is clear from the structure of the fixed-point manifold that a small-amplitude oscillation (${}_0D$), namely oscillation death, is stable for a small parameter value B_1, but this state does not exist for a large parameter value B_1.

[1] B. Barnes and R. Grimshaw, Int. J. Bifurcation Chaos **7**, 2653 (1997).
[2] S. Rajasekar and M. Lakshmanan, J. Theor. Biol. **133**, 473 (1988).
[3] S. Sato and S. Doi, Math. Biosci. **112**, 243 (1992).
[4] B. Braaksma and J. Grasman, Physica D **68**, 265 (1993).
[5] T. Nomura, S. Sato, S. Doi, J. P. Segundo, and M. D. Stiber, Biol. Cybern. **69**, 429 (1993).
[6] A. Rabinovitch, R. Thieberger, and M. Friedman, Phys. Rev. E **50**, 1572 (1994).
[7] T. Nomura, S. Sato, S. Doi, J. P. Segundo, and M. D. Stiber, Biol. Cybern. **72**, 55 (1994).
[8] S. Doi and S. Sato, Math. Biosci. **125**, 229 (1995).
[9] C. Kurrer and K. Schulten, Physica D **50**, 311 (1991).
[10] A. Rabinovitch, R. Thieberger, M. Friedman, and S. Goshen, Chaos Solitons Fractals **7**, 1713 (1996).
[11] A. Rabinovitch and I. Rogachevskii, Chaos **9**, 880 (1999).
[12] K. Shimizu, M. Sekikawa, and N. Inaba, Phys. Lett. A **375**, 1566 (2011).
[13] K. Bar-Eli, Physica D **14**, 242 (1985).
[14] D. G. Aronson, G. B. Ermentrout, and N. Kopell, Physica D **41**, 403 (1990).
[15] I. Shimada and T. Nagashima, Prog. Theor. Phys. **61**, 1605 (1979).
[16] N. Inaba and S. Mori, IEEE Trans. Circuit Syst. **38**, 398 (1991).
[17] M. Sekikawa, N. Inaba, and T. Tsubouchi, Physica D **194**, 227 (2004).
[18] M. Sekikawa, N. Inaba, T. Yoshinaga, and H. Kawakami, IEICE Trans. Fund. Electron. Commun. Comput. Sci. **J87-A**, 199 (2004) (in Japanese).
[19] H. Kawakami, IEEE Trans. Circuit Syst. **31**, 246 (1984).
[20] Y. A. Kuznetsov and I. A. Kuznetsov, *Elements of Applied Bifurcation Theory* (Springer-Verlag, New York, 2004).
[21] T. Yoshinaga and H. Kawakami, *Bifurcation and Chaotic State in Forced Oscillatory Circuits Containing Saturable Inductors* (World Scientific, Singapore, 1995).